Self-Assembly of Block Copolymer Thin Films Having a Half-Domain-Spacing Thickness: Nonequilibrium Pathways To Achieve Equilibrium Brush Layers Parallel to Substrate

Kenji Fukunaga*

Polymer Laboratory UBE Industries, Ltd. 8-1, Goi-minamikaigan, Ichihara, Chiba 290-0045, Japan

Alexander E. Ribbe*,†

Purdue Laboratory for Chemical Nanotechnology, Department of Chemistry, Purdue University, 560 Oval Drive, West Lafayette, Indiana 47907-2048

Takeji Hashimoto*,‡

Advanced Science Research Center, Japan Atomic Energy Agency, Tokai-mura, Ibaraki 319-1195, Japan, and Department of Polymer Chemistry, Graduate School of Engineering, Kyoto University, Katsura, Kyoto 615-8510, Japan

Received January 23, 2006; Revised Manuscript Received May 18, 2006

ABSTRACT: Nonequilibrium processes in thin films of lamella-forming poly(2-vinylpyridine)-*block*-polyisoprene diblock copolymers were studied. The thin films having the half-lamella thickness were prepared by spin-casting of a block copolymer solution onto a hydrogen-terminated silicon wafer (SiH). We found that (1) the as-spun films develop a perpendicularly oriented microdomain structure, i.e., microphase-separated structure with its microdomain interfaces perpendicular to the film surface, and (2) after thermal or solvent vapor treatment, this trapped nonequilibrium structure is transformed into parallel lamellae (lamellar microdomains with their lamella interfaces parallel to the surface) by an orientational transformation process without changing the mean film thickness.

I. Introduction

In this study, we explored the nonequilibrium process in lamellar-forming diblock copolymer thin films, which wet the substrate surface. Particularly, thin films with a half-domain-spacing thickness were studied. Since one block component shows attraction to the free surface and the other the substrate surface, our thin films have the minimum thickness that allows the diblock copolymer to form parallel lamellae. We will show that as-prepared films develop a microphase-separated structure with microdomain interfaces perpendicular to the substrate surface. After thermal or solvent-vapor treatment, this nonequilibrium structure is transformed into monomolecular lamellae with their interface parallel to the substrate surface (parallel lamella having $\sim 1/2$ lamella spacing). We will elucidate the nonequilibrium pathways to achieve the equilibrium structure.

Block copolymers are fascinating materials since they show highly regular microphase-separated structures in mesoscopic dimensions.[1] The interplay of short-range interactions arising from net repulsive interactions between the constituent blocks and long-range interactions arising from the fact that the blocks are covalently bonded at one ends gives rise to a rich variety of ordered microdomain morphologies in the thermal equilibrium. Their morphologies are a consequence of the interplay of the short-range and long-range interactions.[2,3] The microdomain structures have been extensively studied in bulk block copolymers. Recently, however, thin films of these block copolymers attracted much attention due to their potential for use as a template for fabricating various structures on the nanolength scale.[4]

Thin films typically have a thickness less than about 10 times of the spacing of the microphase-separated structure. In such thin films, the constituent blocks encounter distinct short-range interactions arising from the film surfaces (air and substrate surfaces, for example),[5,6] and the geometrical constraints due to the thin film thickness affects the long-range interactions as well. Thus, the interplay is much more enriched in the thin films, which may further enrich the microphase-separated structures within the thin films.[7] As a result of the interplay of these interactions, the component preferred by one surface develops the microdomains on this surface. In the case of a lamella-forming diblock copolymer, this surface selectivity develops a lamella of the one component on the substrate and a lamella of the other component on the free surface. Thus, the selective surface generates a parallel lamellae structure (lamellar microdomains with their lamellar interfaces parallel to the substrate surface) throughout the entire film, although there are some exceptions (thin films on a neutral substrate[8] or on a rough substrate,[9] for example). In a parallel lamellae structure, the local film thickness is adjusted to some quantized values of the lamella spacing. When the substrate surface and the air surface prefer different polymer components of the diblock copolymer, the local film thickness becomes a half-integer ($n + 1/2$) multiple of the lamella spacing d (thickness quantization).[10]

The parallel lamellae structure has been detailed mostly in thermal equilibrium. Although some of the studies extended their

* To whom correspondence should be addressed: K. Fukunaga (28658u@ube-ind.co.jp), A. E. Ribbe (ribbe@purdue.edu), or T. Hashimoto (hashi2@pearl.ocn.ne.jp).

† Part of this work was conducted at the Venture Business Laboratory, Kyoto University, Kyoto 606-8501, Japan.

‡ Present address: Advanced Science Research Center, Japan Atomic Energy Agency, Tokai-mura, Ibaraki Pref. 319-1195, Japan.

10.1021/ma0601666 CCC: $33.50
Published on Web 08/02/2006

Table 1. Molecular Weights and Volume Fractions of Diblock Copolymers Used in This Study

	M_n, 10^3 g/mol	M_w/M_n	vol fraction ϕ_{PI}	vol fraction ϕ_{P2VP}	bulk spacing D, nm
PI-*b*-P2VP-1	183	1.04	0.26	0.74	70
PI-*b*-P2VP-2	67.9	1.31	0.49	0.51	44

scope to nonequilibrium structures that are frequently trapped in thin films during the film preparation procedure or to those that are in the process of their transformation to the parallel lamellae structure, the nonequilibrium process in the thin films is yet not fully understood.

II. Experimental Section

II.1. Samples. Polyisoprene-*block*-poly(2-vinylpyridine) diblock copolymers (PI-*b*-P2VP-1 and PI-*b*-P2VP-2) were synthesized by means of standard living anionic polymerization. The average molecular weight and the volume fractions are presented in Table 1.

Hydrogen-terminated silicon (SiH) substrates were prepared in the following manner: (i) Silicon (111) wafers purchased from Osaka Special Alloy, Japan, were first soaked in a $H_2O/NH_3/H_2O_2$ (4/1/1 v/v/v) mixture at 100 °C for 2 h in order to remove organic impurities. (ii) The wafers were then soaked in a H_2SO_4/H_2O_2 (7/3 v/v) mixture at 100 °C for 2 h for removal of remaining organic impurities and for formation of a thin SiO_x layer. (iii) Finally, the wafers were left in a 1% aqueous solution of HF for 5 min at room temperature to remove the oxide layer. Thin polymer films were prepared on the SiH substrate within 1 day after the final HF treatment.[11]

Two kinds of thin films of PI-*b*-P2VP were deposited on the SiH-terminated substrate by spin-casting at 1800 rpm: one from a 0.13 wt % PI-*b*-P2VP-1 solution and the other from a 0.2 wt % PI-*b*-P2VP-2 solution, both in chloroform. The chloroform solutions were filtered through a microfilter (0.2 mm pore size) prior to use.

Ultrathin films of PI-*b*-P2VP-2 were prepared from PI-*b*-P2VP-2 thin films deposited on a SiH substrate by soaking the thin films in a large amount of chloroform. This procedure removes excess PI-*b*-P2VP chains on the SiH substrate and leaves an ultrathin polymer layer which is strongly adsorbed to the substrate.

Bulk samples of the PI-*b*-P2VP-2 were prepared as follows. A small amount (~1 mL) of the PI-*b*-P2VP solution in chloroform used for spin-casting was put in a vial tube having a small hole that was opened to the air, and thereby the solvent evaporated very slowly (taking more than 2 weeks). Eventually a vitrified polymer film of ~1 mm thickness was obtained in the bottom of the tube. The bulk samples were cut out from the center of the vitrified film.

II.2. Treatment of Thin Films. (a) Heat Treatment. The PI-*b*-P2VP-1 and -2 thin films were annealed under vacuum at a temperature range of 140−210 °C, which is sufficiently higher than the glass transition temperature of both PI and P2VP. After the annealing for given spans, the samples were promptly cooled to room temperature in air.

(b) Solvent Treatment. PI-*b*-P2VP-1 thin films were subjected to the chloroform vapor treatment. The samples were exposed to a saturated chloroform vapor at room temperature for given spans in a sealed glass container. The thin films of the block copolymer were faced to a reservoir of chloroform within 5 mm distance in the container. At the end of the treatment, the samples were taken out of the container and promptly dried.

II.3. X-ray Reflectivity (XRR). X-ray reflectivity (XRR) measurement[12] was used to study the thin film structure of the PI-*b*-P2VP-1. XRR provides information about orientation and roughness of the microdomain interfaces inside the thin films as well as the film thickness. The key parameter of a XRR analysis is the scattering length b or scattering length density b/V, which in turn depends on the electron density ρ_e, which itself depends directly on the mass density ρ:

$$b/V = \rho_e r_0 = \rho N_A n_e r_0 / M_m$$

N_A is Avogadro's constant, n_e the number of electrons per monomer unit, M_m the molecular weight of the monomer unit, and r_0 the length of the monomer. Fitting of the experimental data of XRR with the corresponding electron density profile was done using the recently established standard multilayer fitting routine.[13]

The XRR measurements were done with an X-ray diffractometer SLX 2500K (Rigaku, Tokyo, Japan) operating at 60 kV and 300 mA using a Cu target with Kα line (wavelength $\lambda = 1.54$ Å).

II.4. Transmission Electron Microscopy (TEM). The microphase-separated structure of the bulk PI-*b*-P2VP-2 sample was investigated under transmission electron microscopy (TEM). The samples were ultra-microtomed to about 140 nm thickness and stained by RuO_4 vapor. RuO_4 preferentially stains P2VP, and thereby the P2VP domains appear dark in the TEM pictures. TEM images were taken by JEM-200CX, JEOL, Tokyo, Japan, operated at 100 kV.

II.5. Atomic Force Microscopy (AFM). The surface structures of the thin films were imaged by an atomic force microscope (AFM). A MultiMode AFM with a Nanoscope IIIa controller (Veeco Metrology, Santa Barbara, CA)[14] operated in TappingMode was used for this purpose. Oxide-sharpened silicon cantilevers with a resonance frequency in the 320−340 kHz range and a curvature of some 10 nm were employed for imaging. The sample surface was scanned in the repulsive tip−sample regime, and the ratio A/A_0 of the set point amplitude A to the free oscillation amplitude A_0 was set in the range 0.9−0.97. To minimize a deformation of the PI phase, which is in the rubbery state during the scan, a ratio of A/A_0 close to 1 was chosen. The drive frequency was set such that it caused a 5−15% decrease in the oscillation amplitude, being lower than the resonance frequency. Scan frequency was set in the range 1−2 Hz, providing a stable scan of the sample surface.

II.6. Ultraviolet-Ozone (UV-O_3) Etching. The AFM is straightforward to observe the thin film topographies but reveals only very limited information about the interior of the sample. On the other hand, TEM observations are appropriate to explore the microphase-separated structure inside the thin film but require the removal of the rigid substrate from the thin films and the procedure to cut the removed thin films into ultrathin sections. Since the PI-*b*-P2VP films to be investigated here adsorb very strongly to the substrate, removal of the substrate causes fracture of the thin films and prohibits application of TEM.

Hence, in this study, the microphase-separated structure in the thin films was explored by means of AFM combined with a stepwise etching of the sample surface.[15] Nondestructive interior sensing of elastomers via TappingMode AFM is proposed in the literature.[16] However, since the rigid substrate underneath the thin film sample may give rise to a significant influence on the AFM phase signals inherent in the thin film sample itself, we utilized the aforementioned destructive way as the first step of our study. To etch the sample surface gradually, we utilized an ultraviolet-ozone (UV-O_3) treatment.[17] The samples were placed into a sealed chamber, and subsequently the air in the chamber was purged by oxygen gas. This procedure filled the chamber with high concentrations of oxygen. In the following the samples were illuminated by two UV lamps (one has an emission maximum at $\lambda = 185$ nm and the other at $\lambda = 254$ nm). This UV irradiation decomposes the sample surface and simultaneously forms ozone (originating from the oxygen in the chamber) which also attacks the sample surface. An UV-O_3 cleaner (NL-UV253, Nippon Laser & Electronics Lab., Tokyo, Japan) was used for this purpose. This treatment was found to remove layers of PI-*b*-P2VP off the sample surface in a uniform manner.

Before and after each UV-O_3 treatment the same area was imaged by AFM. To be able to precisely find the same sample position after each etching procedure, distinct scratch marks were made on the sample initially, which allowed a realignment of the etched samples under the microscope.

III. Results

A. Results for PI-*b*-P2VP-1. In this section we start with the results obtained for PI-*b*-P2VP-1. The domain spacing of

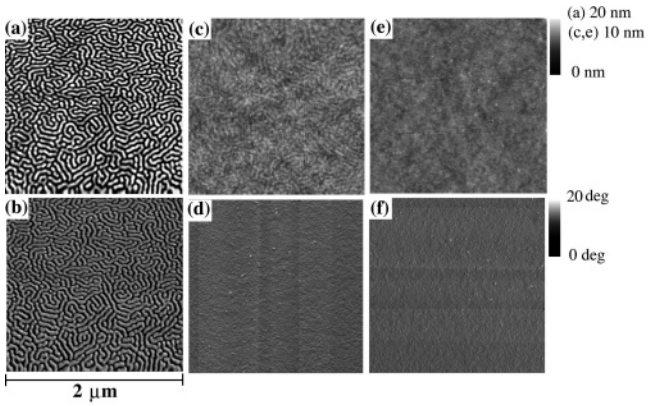

Figure 1. AFM height (top) and phase (bottom) images of PI-*b*-P2VP-1 thin film. Parts a and b show the images of the as-spun film surface. Parts c and d as well as e and f show those for the thin film after the chloroform vapor treatment for 3 and 30 min, respectively.

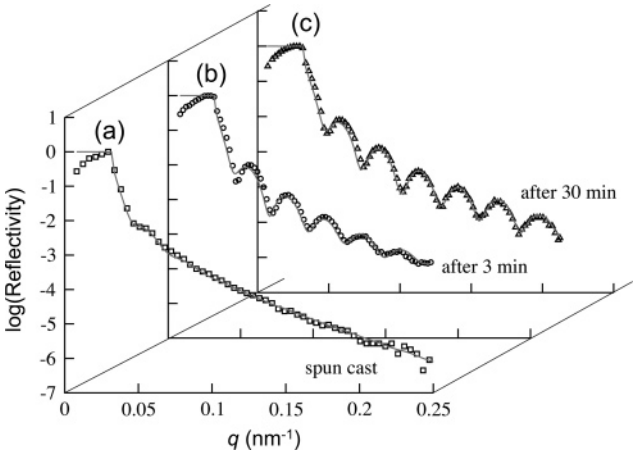

Figure 2. X-ray reflectivity profiles of PI-*b*-P2VP-1: (a) spun-cast from chloroform (open squares), (b) after 3 min (open circles), and (c) after 30 min of the chloroform vapor exposure (open triangles). Curve a−c represent best fits (solid lines) obtained via multilayer fitting routine based on the model described in section IV.4.

bulk PI-*b*-P2VP-1 is 70 nm, which was determined from TEM images observed for ultrathin sections of PI-*b*-P2VP-1 prepared in a manner similar to those of the PI-*b*-P2VP-2 (see section II.1). The thin films with thickness of about 23 nm (slightly less than the half-lamella thickness) were prepared by spin-casting. Figure 1 shows the AFM height (part a) and phase images (part b) of the as-spun film of PI-*b*-P2VP-l. The height image shows that the surface develops a lamellar morphology[18] composed of two microphases: one phase is elevated by about 15 nm relative to the other one. Since the tapping force involved by our AFM measurement is small (see section II.2), such height gap (15 nm) between the P2VP and the PI is not caused only by a deformation of soft PI phase, as will be discussed later in section IV.2.

The contrast of the height image was enhanced by adjusting the gray level differently between image a and images c and e in order to highlight the undulation of the sample surface. The same contrast as the height image is observed in the AFM phase image for the as-spun film as shown in parts a and b. The gray level of the phase image is common for parts b, d, and f in Figure 1 and has not been adjusted differently for each phase image to highlight the contrast. The elevated phase in Figure 1a appears bright on the phase image (Figure 1b), indicating the higher incompressibility of this phase. Therefore, the elevated phase is assessed as the poly(2-vinylpyridine) (P2VP), which is in the glassy state at room temperature. On the other hand, since polyisoprene (PI) is in rubbery state, it is expected to appear darker in Figure 1b. P2VP and PI phase form a lamellar-like morphology on the surface.[18] The average domain spacing in the thin films is about 55 nm, which is determined by the intensity maximum of the circularly averaged two-dimensional Fourier transform of the AFM height image. This spacing is 20% smaller than that of the bulk sample (70 nm), which has been determined for the sample slowly dried from the tetrahydrofuran (THF) solution. This spacing for the as-spun films may be smaller than the equilibrium spacing, since the nonequilibrium structure, which is frequently trapped during the solvent evaporation, in the high molecular weight PI-*b*-P2VP-1 tends to be maintained more firmly than that in the lower molecular weight ones like PI-*b*-P2VP-2. Moreover, the difference of the preparation solvent (chloroform for the thin films and THF for the bulk) in the case of the PI-*b*-P2VP-1 sample may influence the spacing.

The X-ray reflectivity measured for the as-spun film is plotted by open squares (curve a) in Figure 2. The absence of the Kiessig fringes corresponding to the film thickness (23 nm) is possibly due to the large surface roughness arising from the height difference between P2VP and PI phase shown in Figure 1a. The as-spun thin film does not seem to form the parallel lamellae, which are expected to develop Kiessig fringes.

The as-spun film of PI-*b*-P2VP-1 was annealed at 140−200 °C in a vacuum up to 72 h. Although the structure of the as-spun film was not the parallel lamellae and therefore seemed nonequilibrium, the surface topography of the thin film after the heat treatment was not changed (though the AFM data are not shown here), probably because the high molecular weight PI-*b*-P2VP-1 is in the strong segregation regime, so that the microphase-separated structure trapped in the as-spun film may have high kinetic barriers for transformation into parallel lamellae. In recent studies, such nonequilibrium structures have been shown to be successfully transformed into equilibrium structures by the solvent treatment rather than by the conventional heat treatment.[19] Therefore, the solvent treatment of the PI-*b*-P2VP-1 thin film was explored.

Exposure of the PI-*b*-P2VP-1 thin film to the saturated chloroform vapor causes a major change in the film structure as evident from the AFM height images given in parts c and e of Figure 1 which are obtained after 3 and 30 min of the chloroform vapor treatment, respectively. After the vapor treatment for 3 min, the rms surface roughness of the thin film decreased significantly from 4.3 nm to less than 1 nm. The AFM height image in Figure 1c still shows the feature of the lamella-like morphology as the one observed before the solvent treatment (Figure 1a), but the AFM phase image shown in part d lost its contrast. Even if the phase angle range assigned to the gray colors has been reduced to enhance the contrast (not shown here), the contrast of the phase image was hardly observed. After the vapor treatment for 30 min, the AFM height image becomes featureless. Figure 1e shows a maximum height difference of only about 3 nm (rms = 0.54 nm).

The XRR profile recorded after the vapor treatment for 3 min is plotted by open circles (curve b) in Figure 2. In contrast to the case of the as-spun film, the vapor-treated film developed clear Kiessig fringes, increasing substantially in intensity form 3 to 30 min. Since the parallel lamellae are expected to be the equilibrium structure of this system, the appearance of the Kiessig fringes may be related to a parallel lamella formation. Combined with the AFM results shown in Figure 1, the XRR result seems to indicate that a perpendicularly oriented structure (microphase-separated structure with their microdomain inter-

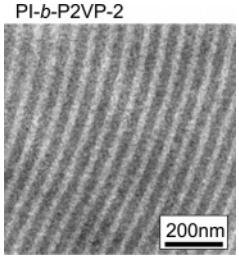

Figure 3. TEM image of the bulk sample of PI-*b*-P2VP-2. The TEM sample has been stained by RuO_4 vapor. PI and P2VP phases appear bright and dark, respectively.

faces perpendicular to the surface) has developed in the as-spun film and was subsequently transformed into the parallel lamellae of the thin block copolymer monolayer with layer interface parallel to the substrate after the solvent-vapor treatment. Since the average film thickness is unchanged during the solvent-vapor treatment, this transformation is an orientational transformation of the microdomain interfaces.

We were strongly inspired by this preliminary result on PI-*b*-P2VP-1 and advanced our study by one step further to explore the details of the nonequilibrium process involved in the orientational transformation in the half-lamella thickness films using a second polymer, PI-*b*-P2VP-2, which has a smaller molecular weight and a more symmetric block composition.

B. Results for PI-*b*-P2VP-2. The solvent sorption and desorption process occurred during the transformation of the PI-*b*-P2VP-1 thin film structure may complicate analyses of the transformation mechanisms.[20,21] To avoid such complexities, we changed the sample to a lower molecular weight PI-*b*-P2VP (PI-*b*-P2VP-2) so that the transformation of the microdomains can be induced only by a conventional heat treatment in a vacuum.

B.1. Bulk Structure. Figure 3 shows a TEM micrograph of the PI-*b*-P2VP-2 bulk sample prepared in the manner described in the Experimental Section. The TEM samples were stained by RuO_4 vapor, which stains the P2VP and PI domains dark and gray, respectively. The micrograph shows that the PI-*b*-P2VP-2 is forming a lamellar structure in bulk. Figure 3 shows an area in which the lamella interfaces are almost perpendicular to the ultrathin sections. The lamella spacing d_{bulk} determined from such TEM pictures is about 44 nm.

B.2. Ultrathin Film. Prior to studying the self-assembly in the half-lamella thickness films of PI-*b*-P2VP-2, we investigated ultrathin films of this copolymer. Here, the ultrathin film designates the monomolecular film of PI-*b*-P2VP-2 on top of the H-terminated silicon substrate. The morphology of these ultrathin films should resemble the structure developed in the first layer of the half-lamella thickness films.[22] Because of the strong adsorption of the P2VP segments to the SiH surface, the PI-*b*-P2VP-2 ultrathin film was obtained by soaking the PI-*b*-P2VP-2 thin film on the SiH substrate in chloroform. After drying the sample a strongly physisorbed brush of PI-*b*-P2VP-2 was observed. Figure 4 shows an AFM height image of this ultrathin film of PI-*b*-P2VP-2. Small protrusions having a bright contrast and their short-range spatial order are observed in the height image. Since these protrusions do not exist on the original SiH substrate, they can only be caused by the ultrathin film. The AFM phase image (not shown here) did not give a sufficient contrast. This is probably because the rigid substrate underneath the very thin film may significantly influence on the phase signal inherent in the structure in the very thin film. Since P2VP blocks are preferentially adsorbed to the substrate, the protrusions are considered to be condensed globules of PI blocks bound to the

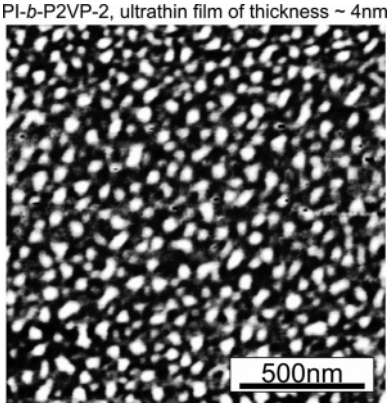

Figure 4. AFM height image of the PI-*b*-P2VP-2 ultrathin film of thickness ~4 nm. The height range of 4 nm is represented by the gray level.

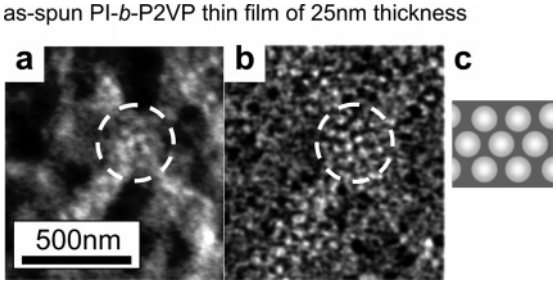

Figure 5. AFM height (a) and phase images (b) of the as-spun PI-*b*-P2VP-2 thin film of 25 nm thickness. The gray level of parts a and b represents a height range of 8 nm and the phase shift range of 10°, respectively. The structure observed in the area indicated by the white circle in parts a and b is schematically drawn in part c. In part c, the bright phase corresponds to P2VP domains protruded in part a and appeared harder in part b.

P2VP blocks on the substrate. They have a characteristic length L_0 (as will be defined later in Figure 8d) of about 63 nm. The thickness of the ultrathin film was determined by the height difference between the film surface and the bare substrate surface, which was artificially induced by scratching the film. The globules have a mean height of about 3 nm measured from the substrate surface, and the area surrounding the globules has thickness ~1 nm.[23]

B.3. Thin Films of a Half-Lamella Thickness. *As-Spun Films.* Figure 5a shows an AFM height image of the as-spun thin film of PI-*b*-P2VP-2. The initial film thickness was $z_0 \approx$ 25 nm, which was again determined by measurement of the step height of the thin film artificially introduced by a scratch as for the case of the ultrathin film above. The height image shows bright round-shaped features on the free surface (see area indicated by the white circle in Figure 5). Therefore, the features slightly protrude (~1 nm) from the surrounding area and have short-range order. The characteristic spacing of these protrusions L_1 (as will be defined later in Figure 8e) is ~63 nm, which is quite similar to the spacing of the protrusions observed on top of the ultrathin film (Figure 4). In the AFM phase image (part b), the protrusions appear as a bright phase. Since the glassy phase appears bright in the phase image, the protrusion and the matrix are considered to be P2VP and PI microdomains, respectively. However, we cannot exclude the possibility that the surface of the protruding P2VP domain is covered by monolayer of PI, which has a lower surface energy than P2VP. The difference of the surface morphology between the PI-*b*-P2VP-1 thin film (Figure 1a,b) and the PI-*b*-P2VP-2 thin film will be discussed in section IV.2.

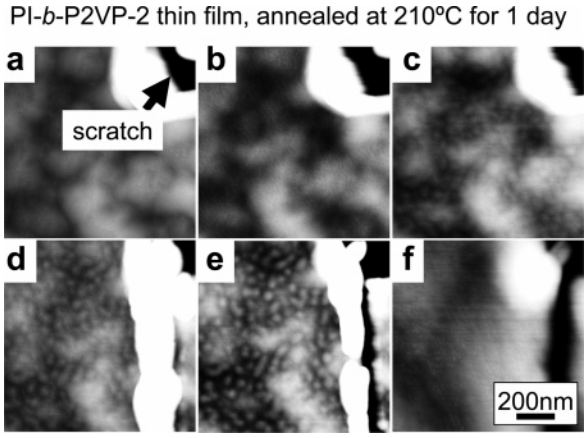

Figure 6. AFM height images of the PI−P2VP-2 thin film after the UV-O_3 treatment of the same area for varying etching thickness Δz: (a) 0 nm (pristine), (b) 1 nm, (c) 7 nm, (d) 11 nm, (e) 16 nm, (f) 19 nm. The scale bar in part f applies to all images. The sample was annealed at 210 °C for 1 day prior to the UV-O_3 etching procedure. The enlargement of the scratch seen in between parts c and d was accidentally caused by the AFM tip during the tip approach toward the sample surface.

After Heat Treatment. The as-spun films of PI-*b*-P2VP-2 were annealed at 210 °C in a vacuum. After the heat treatment for 1 day, the protrusions observed on top of the as-spun film disappeared. At the same time, the surface loses contrast in the AFM phase image (not shown here) as did the as-spun sample PI-*b*-P2VP-1 described earlier. The microphase-separated structure of the as-spun film has transformed into another structure that shows rather featureless surface in the TappingMode AFM measurements.

By stepwise removal of thin layers of polymer from the top of the thin films, the microphase-separated structure in the film becomes accessible to AFM measurements. We concluded that the PI-*b*-P2VP-2 surface can successfully be ablated by the UV-O_3 treatment as detailed in the Experimental Section.

Figure 6 shows a series of AFM height images taken at the same location after the UV-O_3 treatment for various periods. The surface roughness with a considerably large lateral length scale (several micrometers) seen in the AFM images has already existed in the as-spun film. Before the UV-O_3 treatment, the annealed sample shows a rather featureless surface as described earlier (part a). After removal of about 5 nm of polymer via UV-O_3 etching, the surface becomes nonuniform and shows protrusions with a short-range order in the AFM image as shown in part c. As the removed thickness, defined by Δz, increases more than 10 nm, the corrugated morphology becomes more significant, as shown in parts d and e. The surface, however, becomes again featureless when Δz exceeds 20 nm (see for example part f). In other words, the surface becomes uniform again when the remaining thickness is less than 5 nm.

PI-*b*-P2VP-2 has lamella morphology in bulk (Figure 3). Since PI and P2VP are expected to be enriched on the free surface and the substrate surface, respectively, the half-lamella thickness film of PI-*b*-P2VP-2 is supposed to develop a parallel lamella (P2VP half-lamella on the substrate and PI half-lamella on top of the P2VP half-lamella) in the thermal equilibrium. The laterally inhomogeneous morphology inside of the film as evidenced in parts c−e indicates that the parallel lamellae have not been established yet in the thin film. Therefore, heat treatment for 1 day may be insufficient for the sample to attain the thermal equilibrium, and we therefore extended the annealing time.

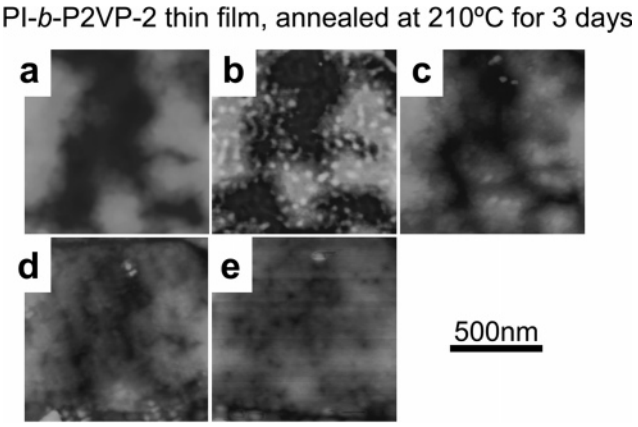

Figure 7. AFM height images of the PI−P2VP thin film annealed at 210 °C for 3 days after the UV-O_3 treatment for various etching thickness Δz: (a) 0 nm (pristine), (b) 8 nm, (c) 14 nm, (d) 18 nm, (e) 19 nm. The scale bar applies to all images.

Figure 7 shows AFM images obtained by the same procedure as described above for the PI-*b*-P2VP-2 thin film after heat treatment at 210 °C for 3 days. Before the UV-O_3 treatment, the thin film surface appears featureless (part a). With the progression of the ablation of the sample surface via UV-O_3 etching, the surface turns to a corrugated surface (part b) and becomes featureless again (parts c−e). Qualitatively, this morphological change in the etched surface is similar to what has been seen in Figure 6. The thickness range, however, in which the corrugated surface is detected, significantly decreased as the annealing time increases. In Figure 6 this short-range ordered structure is observed in an etching depth Δz from 6 to 20 nm. On the other hand, a similar structure (Figure 7) is observed in a more limited Δz range (from about 8 to 14 nm).

IV. Discussion

So far we presented the results for the two different samples, PI-*b*-P2VP-1 and PI-*b*-P2VP-2, separately. In this section we shall first discuss about the results of PI-*b*-P2VP-2 (sections IV.1 to IV.3) and subsequently come back to discuss the more complicated results obtained for PI-*b*-P2VP-1 (section IV.4).

IV.1. Ultrathin Film. Figure 8a reproduces the height image of the ultrathin film shown in Figure 4. The image of the area enclosed by the white broken line in part a is enlarged in part b by converting the gray image into a binary image. The surface topography resembles what has also been observed in PS-*b*-P2VP-*b*-PtBMA[20,21] or PS-*b*-P2VP[24] block copolymers, in which polar P2VP segments are preferentially adsorbed by a native oxide silicon (SiO_x) substrate and the other block forms the condensed globules on top of the P2VP layer. Like a SiO_x substrate, H-terminated Si substrates adsorb selectively P2VP segments. The P2VP chains wet the SiH surface to form the first layer. On top of this first P2VP layer, the PI blocks covalently bonded to the P2VP layer form condensed globules. These PI globules are distributed over the surface of the P2VP layer and are observed as a corrugated surface in AFM height images. In Figure 8b, the binarization threshold has been chosen to be equal to about 1 nm so that the white area represents the PI globule. The PI globules designated by the round markers tend to form hexagons as specified by the solid line on top of the P2VP layer (Figure 8b). Changing the binarization threshold varies the appearance of the image. When the threshold is decreased below 0.9 nm, the white areas start to interconnect. On the other hand, when the threshold is increased over 3 nm, the number of white areas starts to decrease. In the case of the

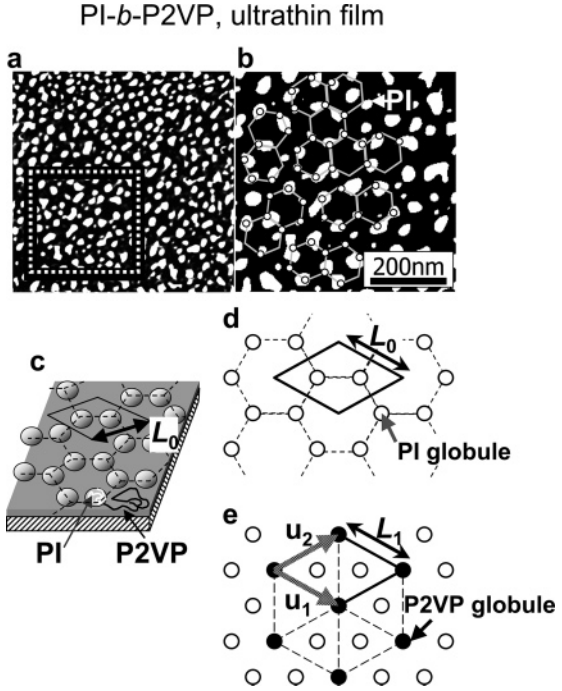

Figure 8. AFM height image of the ultrathin film surface (part a). Part b is a magnification of the area indicated by dotted square in part a and is represented by the binarization so that the PI globules appear bright. Some of the PI globules are highlighted by round markers in part b. Part c represents a schematic model for the structure of the ultrathin film which is comprised of PI globules on the top of P2VP layer adsorbed to SiH. Part d shows the surface unit cell of the ultrathin film by the solid line. A neighboring unit cell is depicted by the broken line in order to represent L_0. Open circles represent the positions of PI globules. Part e shows the surface unit cell of the as-spun thin film. Filled circle represents the P2VP domain positions. $\mathbf{u}_1$ and $\mathbf{u}_2$ represent the surface unit vectors. L_1 and L_0 are anticipated and actually found to be almost identical.

threshold between 0.9 and 3 nm, the characteristic of the spatial distribution of the white areas does not significantly differ from that schematically represented in Figure 8b. A schematic model of the ultrathin film structure is shown in Figure 8c. Although the PI globules have not attained a well-defined long-range order, they seem to be locally ordered in a honeycomb-like pattern as schematically indicated by broken line in part c. The unit cell of this honeycomb structure is depicted by the lozenge of the solid line. Part d schematically represents the unit cell in which the PI globules are marked by the open circles. The edge length L_0 of the unit cell is ~63 nm as determined from the AFM images, which will be discussed in the next section (Figure 8e).

IV.2. Thin Films of a Half-Lamella Thickness. As shown in Figure 5, the free surface of the as-spun films exhibits P2VP domains having a short-range order in the PI matrix. The P2VP domains are protruded relative to the surface of the PI matrix. We interpret the P2VP protrusions as follows. The solvent (chloroform) used for the film preparation is common solvent for both PI and P2VP. Since the glass transition temperature of P2VP is significantly higher than that of PI, the P2VP phase is vitrified earlier than the PI phase during the solvent evaporation. After the vitrification of the P2VP domains, the PI domains further shrink as the residual solvent evaporates. It is therefore quite reasonable to observe the protruded P2VP domains on the surface of the as-spun films, giving rise to a depression of the PI domain surface relative to the P2VP domain surface.

Most likely the P2VP phase is covered by a thin PI monolayer, since this is energetically favorable. Depending on

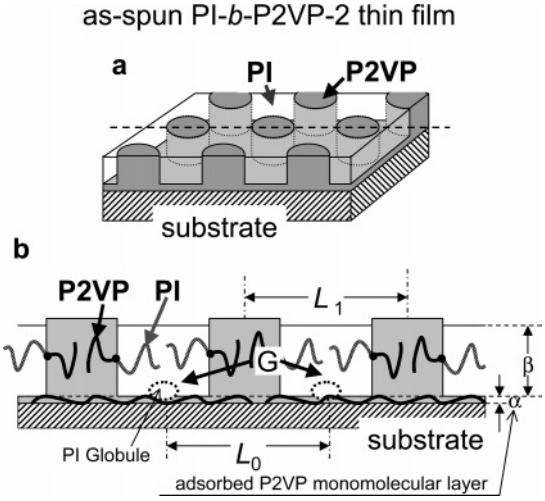

Figure 9. (a) Schematic model of the as-spun thin film structure. Part b displays a cross-sectional view of the model cut through the plane including the broken line shown in part a, which is parallel to $\mathbf{u}_1$ in Figure 8e. In part b, α and β schematically designate the P2VP monomolecular layer and the second layer comprised of PI and P2VP blocks on the top of the first molecular layer, respectively. Although the PI globules (G) are not in this cross-sectional plane, their projection on the same plane is represented. L_0 and L_1 represent the characteristic length for the unit cell of the PI globules and that of the P2VP domains defined in parts d and e of Figure 8, respectively. $L_1 \approx L_0 \approx 63$ nm was found experimentally in our system.

thickness of the soft PI monolayer which covers the glassy P2VP domain, the TappingMode AFM tip dissipates energy and thereby varies the phase signal.[16] As a result, the AFM phase image exhibits contrast shown in Figure 5b.

The characteristic spacing of the protruded P2VP domains L_1 observed on top of the film in Figure 5 is very similar to the unit cell length of the PI globules L_0 observed on top of the ultrathin film (see Figure 8d, section IV.1). The spacing L_0 of the PI globules is determined by the spatial distribution of the junction points between PI globules on the first layer of P2VP, as shown in Figure 9 (the layer α). The junction points have a high kinetic barrier to move due to the strong interactions between the P2VP segments and the substrate surface and hence due to stiffness of the P2VP layer. In the PI-*b*-P2VP-2 films of about 25 nm thickness too, the spatial distribution of the junction points in the first P2VP layer is believed to be almost the same as in the ultrathin film structure. Therefore, we may consider the following model represented by Figure 9 for the structure of the as-spun thin film.

The condensed PI globules form on top of the physisorbed layer of P2VP, as described in section IV.1. The spatial distribution of the PI globules on top of the first P2VP monomolecular layer (layer α in Figure 9) seems to have short-range order characterized by a unit cell, as represented in Figure 8d. In the second or higher molecular layer (layer β in Figure 9), the P2VP chains are expelled from the position occupied by the PI globules in the first molecular layer in order to minimize the unfavorable contact between PI phase and P2VP phase. The P2VP chains therefore segregate into the complementary space in the second or higher layer with respect to the PI globule (G), as represented in Figure 9b and in the unit cell shown in Figure 8d. These positions for the centers of the P2VP domains, together with the unit cell of the surface structure of the first molecular layer surface, are schematically indicated by filled circles in Figure 8e. The center of the P2VP phase is expected to be located in the corner of the unit cell of the PI globules and thereby to form the close-packed hexagonal

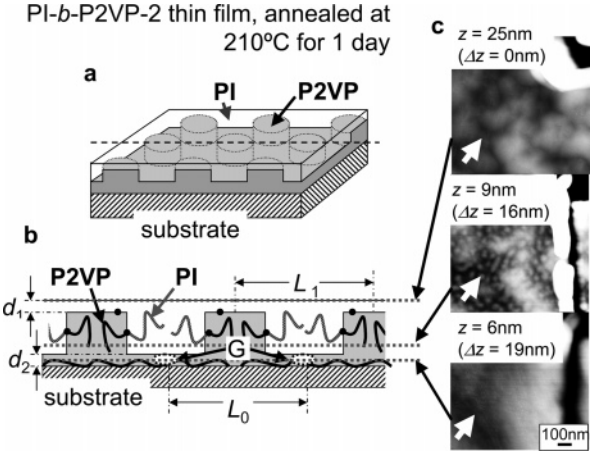

Figure 10. Schematic model of the thin film structure after annealing at 210 °C for 1 day (part a). Part b displays a cross-sectional view of the model cut through the plane including the broken line in part a, which is parallel to $\mathbf{u}_1$ in Figure 8e. The dark dots on the interface denote chemical junction points of the block copolymers. Part c reproduces the AFM height images recorded at the height indicated by the broken lines in part b. The characteristic spacing of the P2VP domain (L_1) is unchanged compared to the as-spun film. Although the PI globules (G) are not in this cross-sectional plane, their projection is represented in the same plane. For other markers, see Figure 9. Though PI and P2VP chains in the first and second molecular layer or in the second and the higher molecular layer may interpenetrate each other, the boundary of the respective molecular layer are represented simply by the broken lines here.

structure. Further, the characteristic spacing L_1 between the P2VP domains, which perforate the PI domains and appear on the free surface, is expected to become almost identical to that of L_0 for the unit cell size of the PI globule arrays (Figure 8c,d) in the ultrathin films, as demonstrated in Figure 9b. Indeed, the as-spun film surface shows the close-packed hexagonal structure of the P2VP domains, and the characteristic distance between the P2VP domains is the same as the 63 nm observed for the unit cell size of the ultrathin film surface structure. These P2VP domains may be considered as the P2VP cylinders standing up with respect to the special layer α in Figure 9, although the polymer forms the lamellae in bulk. The apparent difference in the morphology of the as-spun film surface of PI-*b*-P2VP-2 (Figure 5) and PI-*b*-P2VP-1 (Figure 1a,b) is considered to come from the difference in composition of the block copolymers. While the PI-*b*-P2VP-2 has the nearly symmetric volume fraction, the P2VP volume fraction is considerably large in PI-*b*-P2VP-1. Thereby, the P2VP forms cylinders in the PI-*b*-P2VP-2 thin films in contrast with the layers in the PI-*b*-P2VP-1 thin films.

After the thermal treatment, this nonequilibrium structure that has been trapped and frozen during the film preparation process is transformed into its equilibrium morphology. The disappearance of the surface corrugation after the heat treatment at elevated temperature seems to indicate formation of laterally homogeneous layer on top of the thin film, as illustrated in Figure 10b. Since PI has a lower surface energy than P2VP, the PI chains in the PI microdomain in Figure 9 are transformed to cover the free surface of the thin film, as shown in Figure 10b. Eventually, a thin layer of PI covers the surface of the P2VP domains. Although this process tends to flatten the free surface, the microdomain interfaces perpendicular to the film surface still exist in the middle of the thin film. The process should involve translational diffusion of the junction points along the microdomain interface, as will be detailed in section IV.3.

Figure 10c shows the AFM height images acquired after the UV-O_3 etching of the thin film to the height indicated by the broken lines in part b. At $\Delta z \approx 16$ nm the etched surface exhibits laterally inhomogeneous structures, which show a characteristic spacing similar to the surface corrugation of the as-spun film. In contrast to the case at $\Delta z \approx 16$ nm, the free surface at $\Delta z \approx 0$ nm and the surface etched at 19 nm show a featureless surface topography. The etched surface at $\Delta z \approx 16$ nm intersects the microdomain interfaces that are perpendicular to the film surface. Hence, this surface appears as a laterally inhomogeneous surface topography in the AFM image. In comparison, the surfaces at $\Delta z \approx 0$ and 19 nm do not intersect the microdomain interface. Therefore, the AFM images appear featureless. The height range at which the etched surface intersects the microdomain interfaces is in the range of 20 nm $> z >$ 6 nm (initial thickness $z_0 \approx 25$ nm) after the heat treatment at 210 °C for 1 day, as described in subsection B.3 in section III.

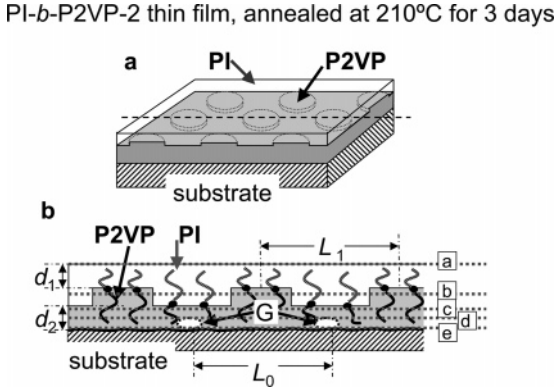

Figure 11. Schematic model of the thin film structure after annealing at 210 °C for 3 days (part a). Part b displays a cross-sectional view of the model cut through the plane including the broken line shown in part a, which is parallel to $\mathbf{u}_1$ in Figure 8e. The levels labeled by a−e correspond to the height of parts a−e in Figure 7. The characteristic spacing of the P2VP domain (L_1) is unchanged from that of the as-spun film. For other markers, see Figure 9.

After the extended heat treatment at 210 °C for 3 days, the microdomain structure in the thin film was further transformed toward an equilibrium structure. Although thin films of PI-*b*-P2VP-2 after the heat treatment for 1 day (Figure 6) and that after 3 days (Figure 7) show qualitatively similar trends during the UV-O_3 treatment, the height range in which the ablated thin film surface intersects the microdomain interfaces for the specimens after 3 days (Figure 7) is significantly narrower than that for the case after 1 day (Figure 6). The model of the microdomain structure explaining the result of Figure 7 is schematically depicted in Figure 11. The height levels labeled by a−e in Figure 11b correspond to the heights of the surface (or etched surface) observed in part a−e of Figure 7. Level b intersects the perpendicular microdomain interface and thereby exhibits a laterally inhomogeneous morphology in the corresponding AFM height image (Figure 7b). Although the undulated microdomain interfaces between the PI and P2VP phases still exist, the amplitude of the undulations in the direction perpendicular to the film surface decreases considerably after the prolonged heat treatment of 3 days (see Figure 11) in comparison to the shorter heat treatment of 1 day (see Figure 10). More accurate determination of the change in the interface position during the heat treatment may be possible by detailed analysis of the AFM phase image with harder tapping conditions.[16]

IV.3. Mechanism of Transformation: Nonequilibrium Pathway. In the PI-*b*-P2VP-2 thin films, PI is located at the free surface and the more polar P2VP at the substrate surface.

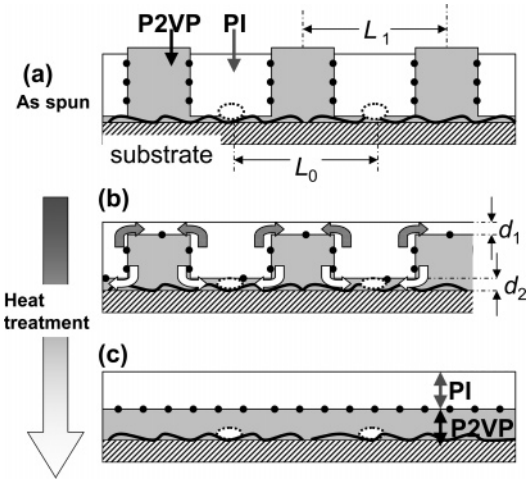

Figure 12. Schematic diagram visualizes the transformation mechanism of the PI-*b*-P2VP thin film structure during the heat treatment: (a) as-spun state, (b) intermediate state, and (c) the equilibrium state. The black dot on the microdomain interfaces schematically represents the junction point between the PI block and the P2VP block. After the heat treatment, some of the junction points on the microdomain interfaces perpendicular to the substrate are moved on the interface parallel to and close to the substrate surface as indicated by the brighter arrows, and some of the junction points are moved on the interface parallel to and close to the free surface as indicated by the dark arrows. A depression of the parallel interface in the air side by the height d_1 is compensated by an elevation of the parallel interface (in the substrate side) by the height d_2 in such a way that the volume conservation is satisfied. Eventually, the microdomain interfaces perpendicular to the film surface that have developed in the as-spun film are transformed into the interface parallel to the film surface.

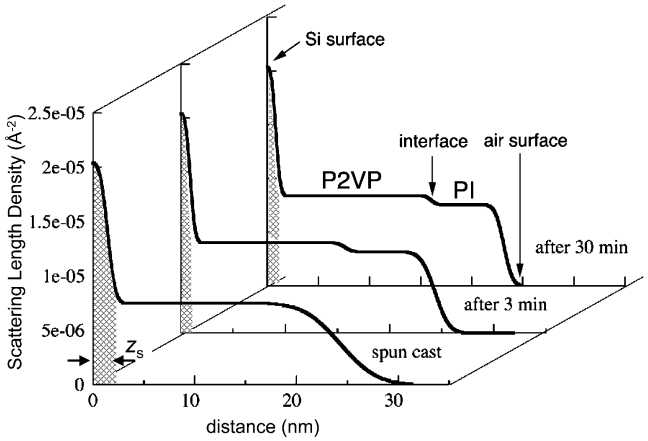

Figure 13. One possible set of density profiles along the substrate normal as determined from XRR profiles. The model used is based on the model shown in Figure 12, which is constructed from the morphologies derived by the UV-O_3 etching and AFM experiments (section IV.2). The scattering length density increased in the cross-hatched portions due to the contribution of the SiH substrate and/or the special surface structure arising from the physisorbed P2VP layer as discussed in section IV.1.

The PI-*b*-P2VP will therefore most likely develop a parallel lamella structure (lamellae with their interfaces parallel to the film surface) in the thin film, by forming PI-half-lamella on the free surface and P2VP-half-lamella on the substrate surface. Although the microphase separation of PI and P2VP seems to be accomplished locally, the as-spun film as a whole does not attain the parallel lamella structure. When the film thickness is thinner than the half-lamella spacing, formation of the parallel lamellae is suppressed and thereby perpendicular lamellae are formed. In this work, however, the film thickness z_0 is chosen to be about the half-lamella thickness $d_{bulk}/2$, and therefore the parallel lamellae formation is believed to be not restricted by the film thickness.

The special adsorbed layer structure discussed in section IV.1 develops on the substrate surface. A transformation of this structure with the heat treatment is expected to have a high kinetic barrier due to the strong interactions between the P2VP and the substrate surface, and hence the structure is expected to be conserved with the annealing. As discussed in section IV.2, however, the adsorbed layer structure seems to strongly influence the structure of the whole as-spun film. The special structure on the substrate may give rise also to the kinetic barrier to the equilibration of the microdomain structure in the entire film.

We propose the equilibration mechanism or process as schematically depicted in Figure 12. Through heat treatments for the prolonged time periods or the solvent vapor treatment, the nonequilibrium microdomain structure is transformed to the parallel lamellae by the way of decreasing area of the microdomain interface perpendicular to the film surface. The process involves translational diffusion of chemical junctions of the block copolymers along the planar interface oriented perpendicular to the thin film toward the interfaces parallel to the substrate surface, as shown by the gray and white arrows in part b. The diffusion creates new PI layers having thickness d_1 in the air side and new P2VP layers having thickness d_2 on the top of the first layer α defined in Figure 9. Since the surface area parallel to the substrate does not change with the heat treatments, the transformation process tends to decrease total interfacial area and hence to stretching the block chains normal to the interface, which is a natural trend for the equilibration process.[25]

The undulated microdomain interfaces developed in the as-spun film gradually decrease the amplitude of the undulation in the direction normal to the film surface with the annealing time. This process did not change the characteristic wavelength of the undulation in the direction parallel to the film surface as evidenced by the constant spacing L_1. A PI-*b*-P2VP half-lamella structure is supposed to be established in the thin film after very long annealing time, although our experiment has not reached this state yet. However, even if sufficiently long annealing is applied to the thin films, the special structure on the substrate surface may give rise to some undulation to the interface between P2VP lamella and PI lamella.

IV.4. Revisit of XRR Results. On the basis of the model shown in Figure 12, the XRR results shown in Figure 2 are converted to density profiles. A one-layer model was used for the as-spun film, and a bilayer model was applied for the samples after the solvent vapor exposure. In the one-layer model, the contribution of the layer α to the XRR results was incorporated as the roughness of the substrate surface. The best fit of the XRR results was achieved by the density profiles shown in Figure 13, and the fitted XRR results are represented by the solid curves in Figure 2. The roughness of the substrate surface is represented by the thickness of the crosshatched area z_s in Figure 13, though roughness z_s of the as-spun film is thicker than those after the solvent-vapor treatments. Since the SiH surface roughness does not change by the solvent vapor treatment, this apparent increase in z_s of the as-spun film seems to indicate the formation of the special structure on top of the substrate (layer α in Figure 9). The density of the layer α is possibly higher than that of the rest part of the film due to the strong adsorption of the P2VP to the substrate surface. The film thickness and the preferential adsorption of the certain component of the block copolymer to the substrate play a crucial role to the perpendicular morphology, as previously shown in the

thin films of PS-*b*-PMMA,[26] PS-*b*-P2VP-*b*-PMMA, and PS-*b*-PHEMA-*b*-PMMA[27] on polar substrates.

The density profiles after 3 and 30 min of the chloroform vapor treatment are not significantly different. It indicates that the PI-*b*-P2VP-1 thin film almost attained the final state of the orientational transformation process as shown in the bottom of Figure 12 after 3 min of the chloroform vapor treatment. The time scale of the transformation is considerably shorter than the case of the heat treatments of the PI-*b*-P2VP-2 thin films. In the case of the vapor treatment, the transformation in the PI-*b*-P2VP thin films is expected to proceed much faster than in the case of the conventional heat treatment due to the significant decrease in the glass transition temperature of the polymer chains in the thin film swollen by the solvent.

V. Conclusion

In this study, we investigated the microphase-separated structure of the lamella-forming PI-*b*-P2VP diblock copolymer in the thin films having the half-lamella thickness. Because of the preferential segregation of the P2VP (PI) to the substrate surface (air surface), the diblock copolymer used in this work forms the parallel lamella structure in the thermal equilibrium. The as-spun films, however, were elucidated to develop the P2VP microdomains protruded on the film surface in the PI matrix. The spatial distribution of the P2VP microdomains appearing on the free surface showed only short-range order. The ultrathin films (monomolecular films) of the corresponding diblock copolymer also showed the short-range ordered morphology, but in this case the PI globules are protruded on top of the P2VP layer adsorbed to the substrate surface. The characteristic spacing of the P2VP microdomains L_1 in the half-lamella thickness films is quite close to that of the PI globules L_0 in the monomolecular films, indicating that the distribution of the P2VP microdomains in the half-lamella thickness films is considerably influenced by the configuration of the P2VP chains adsorbed on the substrate surface. After the thermal treatment, the trapped nonequilibrium structure of the as-spun films has been transformed into parallel lamellae by the orientational transformation process without significantly changing the film thickness. The latter process involves translational diffusion of the junction points of the block copolymer along the interface, such that the interface oriented perpendicular to the substrate is diminishing with time, keeping the total interfacial area parallel to the substrate and air surface constant. This implies the total interfacial area decreases with time and hence invariably increases interfacial area density of the junction points of the block copolymers (number of the block copolymer chains per unit area of the interface), resulting in chain stretching.

Acknowledgment. A.R. is grateful to Dr. Kazumi Matsushige for his support and encouragements of XRR experiments during his time at the Venture Business Laboratory, Kyoto University.

References and Notes

(1) Hamley, I. *Physics of Block Copolymers*; Oxford University Press: Oxford, 1998; Vol. 94.
(2) Hashimoto, T.; Yamauchi, K.; Yamaguchi, D.; Hasegawa, H. *Macromol. Symp.* **2003**, *201*, 65.
(3) Hashimoto, T.; Yamaguchi, D.; Court, F. *Macromol. Symp.* **2003**, *195*, 191.
(4) Park, M.; Harrison, C.; Chaikin, P. M.; Register, R. A.; Adamson, D. H. *Science* **1997**, *276*, 1401.
(5) Russell, T. P.; Coulon, G.; Deline, V. R.; Miller, D. C. *Macromolecules* **1989**, *22*, 4600.
(6) Coulon, G.; Deline, V. R.; Green, P. F.; Russell, T. P. *Macromolecules* **1989**, *22*, 2581.
(7) Hasegawa, H.; Hashimoto, T. *Macromolecules* **1985**, *18*, 589. Hasegawa, H.; Hashimoto, T. *Polymer* **1992**, *33*, 475.
(8) Huang, E.; Mansky, P.; Russell, T. P.; Harrison, C.; Chaikin, P. M.; Register, R. A.; Hawker, C. J.; Mays, J. *Macromolecules* **2000**, *33*, 80.
(9) Sivaniah, E.; Hayashi, Y.; Matsubara, S.; Kiyono, S.; Hashimoto, T.; Fukunaga, K.; Kramer, E. J.; Mates, T. *Macromolecules* **2005**, *38*, 1837.
(10) Coulon, G.; Ausserre, D.; Russell, T. P. *J. Phys. (Paris)* **1990**, *51*, 777.
(11) Some reoccurring growth of the native oxide on the SiH may have happened under ambient conditions, although the oxidation rate is very slow. See e.g.: Bodlaki, D.; Borguet, E. *J. Appl. Phys.* **2004**, *95*, 4675.
(12) Russell, T. P. *Mater. Sci. Rep.* **1990**, *5*, 171.
(13) Welp, K. A.; Co, C. C.; Wool, R. P. *J. Neutron Res.* **1999**, *8*, 37.
(14) Magonov, S. *Handbook of Surfaces and Interfaces of Materials*; Nalwa, H. S., Ed.; Academic Press: San Diego, CA, 2001; Vol. 2, pp 393−430.
(15) Magerle, R. *Phys. Rev. Lett.* **2000**, *85*, 2749.
(16) Bodiguel, H.; Montes, H.; Fretigny, C. *Rev. Sci. Instrum.* **2004**, *75*, 2529.
(17) Maeda, K. *Kurin Tekunoroji* **1995**, *5*, 45.
(18) Although one may also argue that the morphology can be seen as lying cylinders, we model this morphology by lamellae as the first approximation. As will be shown in section IV.4, the lamella model can successfully explain the XRR results.
(19) Fukunaga, K.; Hashimoto, T.; Elbs, H.; Krausch, G. *Macromolecules* **2002**, *35*, 4406.
(20) Kim, G.; Libera, M. *Macromolecules* **1998**, *31*, 2569; *Macromolecules* **1998**, *31*, 2670.
(21) Fukunaga, K.; Elbs, H.; Magerle, R.; Krausch, G. *Macromolecules* **2000**, *33*, 947.
(22) Fukunaga, K.; Hashimoto, T.; Elbs, H.; Krausch, G. *Macromolecules* **2003**, *36*, 2852.
(23) The lateral diameter of the PI globule appears to be some 50 nm. Because of tip convolution effects, the actual globule is smaller than this size. If we regard the PI globule as a column having a 25 nm diameter and a height of 2 nm on top of the P2VP layer of 1 nm thickness, the volume of the globule is 4000 nm^3. Since the volume of one PI-block chain of PI-*b*-P2VP-2 is 54 nm^3, the single globule is expected to contain 74 PI-block chains. Total volume of 74 P2VP block chains connected to the PI globule is 4200 nm^3, and it is comparable to the volume of the 1 nm thickness with 4200 nm^2 area. This area is quite similar to the unit cell size with the characteristic length (L_0) of 63 nm (defined in Figure 8d).
(24) Spatz, J. P.; Sheiko, S.; Moeller, M. *Adv. Mater.* **1996**, *8*, 513.
(25) Hashimoto, T.; Shibayama, M.; Kawai, H. *Macromolecules* **1983**, *16*, 1093.
(26) Morkved, T. L.; Jaeger, H. M. *Europhys. Lett.* **1997**, *40*, 643.
(27) Böker, A.; Müller, A. H. E.; Krausch, G. *Macromolecules* **2001**, *34*, 7477.

MA0601666